Check for updates

Band gap engineering and photoluminescence tuning in halide double perovskites

Sergei A. Novikov, [ID] † Aleksandra D. Valueva [ID] † and Vladislav V. Klepov [ID] *

Halide double perovskites (HDPs) present a convenient alternative to the unstable and toxic lead halide perovskites for various optoelectronic applications. Because of their compositional and structural tunability, many HDP phases have been synthesized in the past decades. While efficient photovoltaic applications remain largely out of reach for the HDP phases due to their wide band gaps and structures with pseudoisolated metal centers, their electronic structures favor light conversion applications. Since the field of HDP witnesses rapid growth and development, this article is aimed at providing a brief snapshot of the recent advances on all-inorganic HDPs, primarily focusing on the relationship between their compositions and optical properties, and some aspects of their applications for visible light conversion.

1. Introduction

$A_2M'^{+}M''^{3+}X_6$ halide double perovskite (HDP) and $A_2M^{4+}X_6$ vacancy-ordered HDP bulk powders, thin films, micro- and nanocrystals attract a great deal of interest owing to their broad compositional tunability and valuable optoelectronic properties.[1–7] One of the main advantages of HDPs that have made them attractive for optoelectronic applications is the ability to relatively simply tune their band gap to match the desired spectral range and achieve a high absorption efficiency in the UV-visible range. While it is not uncommon for pristine materials to demonstrate unsatisfactory intrinsic properties due to indirect band gaps or parity-forbidden electronic transitions,[8–10] a wide compositional tunability of HDPs comes in handy. Alloying and doping are efficient and versatile strategies that are commonly employed to tune the band gap and electronic structures. Although most HDPs are characterized by a wide band gap, hindering their photovoltaic applications,[3,11] the remarkable composition tunability grants them photoluminescent emission wavelengths covering the entire visible-near IR range.[12–19] Such materials can be employed as white light emitting phosphors for general lighting applications and have many advantages over commonly used multicomponent phosphor-converted white LEDs based on lanthanide elements. For example, a single matrix luminescent material neither requires precise mixing with other components to achieve optimal performance nor suffers from reabsorption and uneven degradation rates of different components of a multicomponent scheme.[20–23]

Due to the undimmed interest in HDPs, including lead-free hybrid organic–inorganic halides, there have been many reviews on the engineering of properties in these phases.[24–26] In this brief review, we focus on the most recent examples of tuning of the optical properties of all-inorganic HDP materials. We also seek to navigate the readers through the multitude of compositional changes in HDP phases for the desired properties and applications. We consider the effects of alloying and doping from two interrelated perspectives vital for light conversion: one focuses on the change of band structures and the band gap, whereas the other addresses the impact of doping on photoluminescence (PL). While some dopants affect one aspect of the electronic structure, others can be used to both tune the electronic structure and act as a luminescence center simultaneously. Various dopants are employed to achieve efficient broadband emission either through breaking of wavefunction parity or through introducing new luminescence centers in the HDP matrix.[27–36] The effects of common dopants, such as transition metals (TM), rare-earth metals (RE), elements with ns^2 electron configuration and the different combinations of them, are reviewed in this paper.

2. Band gap and band structure tuning

Halide double perovskites can be broadly divided into two classes, direct and indirect band gap materials. The most ubiquitous examples of indirect band gap double perovskites are $Cs_2AgBiCl_6$ and $Cs_2AgBiBr_6$, which have low absorption coefficients and photoluminescence quantum yields (PLQYs) due to

Department of Chemistry, University of Georgia, 302 East Campus Road, Athens, GA 30602, USA. E-mail: klepov@uga.edu

† These authors contributed equally.

the simultaneous involvement of both photons and phonons in the excitation and recombination processes, increasing the probability of a non-radiative relaxation.[10] The valence band maximum (VBM) of $Cs_2AgBiBr_6$ with E_g = 2.87 eV originates primarily from the Ag-4d and Br-4p orbitals, whereas the conduction band minimum (CBM) is mainly derived from the antibonding states of Ag-5s and Bi-6p.[10] The indirect band gap nature of this compound is due to the VBM, which is located at the X point of the Brillouin zone, while the CBM is at the L point (Fig. 1).[10]

A direct band gap is characteristic of compounds such as $Cs_2AgInCl_6$ and $Cs_2AgSbCl_6$, which demonstrate high absorption coefficients and increased PLQYs.[37] $Cs_2AgInCl_6$ has a band gap of approximately 3.1 eV at the Γ point.[37] While the VBM primarily originates from the hybridized antibonding Ag-4d and Cl-3p orbitals, the rest of the valence band is mainly contributed by more localized In-5s and 5p orbitals. The CBM mainly derives from the delocalized In-5s states, which have a large dispersion and a low effective mass.[37] The VBM and CBM of $Cs_2AgInCl_6$ have the same parity (even) at the Γ point,

which makes the direct optical transition forbidden by the selection rule.[37]

Doping and alloying of the double perovskites with group 13 and group 15 elements are the most common strategies for tuning the band structure and band gap of these materials (Fig. 2). Convenient band gap tuning without changing its nature can be achieved *via* preparation of solid solution series with isovalent cations. In $Cs_2AgBiBr_6$, Bi^{3+} cation substitution with Sb^{3+} reduces the band gap in a relatively narrow range from 2.27 eV to 1.80 eV for 0 and 33% of Sb^{3+}, respectively.[38] Curiously, the Sb^{3+} substitution level is limited by the structural stability of the octahedral units and the formation of a secondary phase, revealing some limitations of this approach for band gap tuning.[38]

Unlike isovalent substitution that often causes a gradual change in the band structure, aliovalent substitution can introduce new levels and shift the Fermi level. For example, Sn^{4+} incorporation into the $Cs_2AgBiBr_6$ double perovskite matrix results in lowering of the band gap due to the formation of a new band by hybridization of Sn-5s and Bi-6p orbitals.[39] As a result, the band gap reduces by 0.2 eV due to lowering of the CBM. Ge^{4+} incorporation into the Bi site has a similar effect to Sn^{4+} substitution, but the band gap reduction is smaller, 0.1 eV, because of the smaller radius of the Ge-4s orbital, resulting in a weaker overlap with the Bi-6p orbitals.[39]

A dramatic band gap narrowing from 3.19 eV to 1.24 eV is reported for $Cs_2NaInCl_6$ by introducing Sb^{5+} doping.[40] The authors claim that the $[SbCl_6]^-$ cluster formation within the crystal lattice generates a localized insertion energy band between the VB and CB. This new level contributes to band gap narrowing as evidenced by strong visible light absorption.[40] However, this interpretation is challenged in a recent comment by Xiao, who argues that the observed band gap narrowing is likely due to the formation of a side product $Cs_4Sb^{III}Sb^VCl_{12}$ rather than the intrinsic properties of the doped $Cs_2NaInCl_6$ material.[41]

Isovalent cations from different groups act similarly to the aliovalent ones and change both the position of the Fermi level and band dispersion. In $Cs_2Ag_xNa_{1-x}Bi_yIn_{1-y}Cl_6$, the band gap decreases from 3.12 eV for y = 0.0005 to 2.68 eV for y = 1.[42] The valence band edge shifts to lower energies as the Bi content increases, from 2.66 eV for y = 0 to 1.75 eV for y = 1 with respect to the Fermi level. The conduction band edge also shifts to lower energies as the Bi content increases, following the band gap narrowing. These changes in the band structure
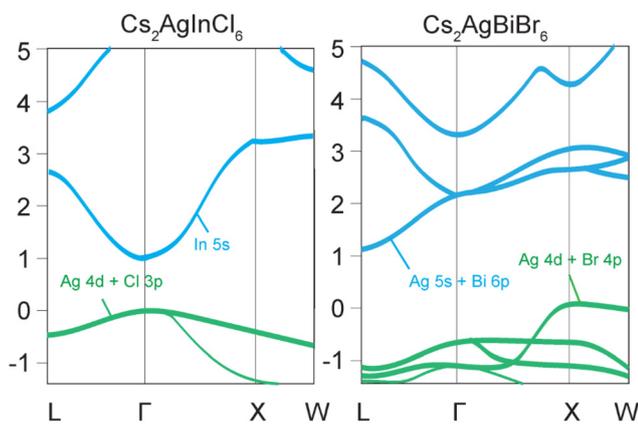

Fig. 1 Schematic illustration of direct and indirect band gaps of halide double perovskites. (Left) In the direct band gap HDP $Cs_2AgInCl_6$, both valence band maximum (VBM) and conduction band minimum (CBM) are located at the Γ point. The VBM is due to hybridization of Ag-4d and Cl-3p orbitals, whereas the CBM is mainly contributed by In-5s orbitals. (Right) $Cs_2AgBiBr_6$ is a typical indirect band gap HDP with the VBM contributed by Ag-5s and Bi-6p orbitals, and the CBM by Ag-4d and Br-4p orbitals.

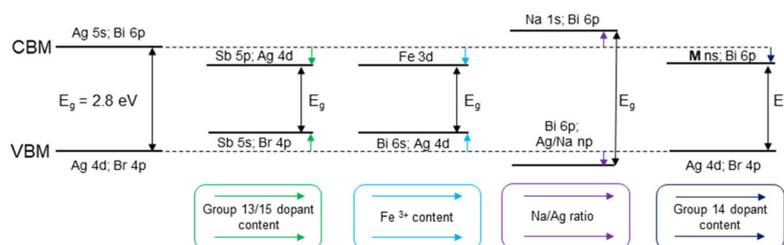**Fig. 2** Effect of the substitution on the conduction and valence bands and the band gap in $Cs_2AgBiBr_6$ HDPs.

are attributed to the introduction of $[BiCl_6]^{3-}$ units into the $Cs_2Ag_xNa_{1-x}Bi_yIn_{1-y}Cl_6$ lattice, which break the symmetry and create localized states below the conduction band minimum, thus facilitating light absorption and emission.[42]

Transition metal (TM) ion incorporation has also been probed as a relatively uncommon yet effective way of band gap engineering in halide perovskites. The band gap of $Cs_2AgBiBr_6$ can be reduced from 2.2 eV to 1.8 eV after 25% Ru-doping, as calculated by DFT.[43] A new intermediate band, dominated mainly by Ru 4d orbitals, appears within the original band gap of $Cs_2AgBiBr_6$. The intermediate band lies below the Fermi level and offers additional transition channels to the conduction band.[43] In another example, $Cs_2AgIn_xFe_{1-x}Cl_6$ ($0 \leq x \leq 1$), the band gap has been tuned by varying the In content, from 0.21 eV for $x = 0$ to 0.72 eV for $x = 1$.[44] Both $Cs_2AgFeCl_6$ and $Cs_2AgInCl_6$ have a direct band gap, while the mixed $Cs_2AgIn_{0.76}Fe_{0.24}Cl_6$ phase exhibits an indirect one, requiring a phonon assistance for an electron transition. The CBM, which is composed of In-5s states, remains largely unchanged in the entire composition range.[44] However, Fe incorporation changes the VBM from being primarily contributed by Cl-3p and Ag-4d states to Fe-3d and Cl-3p, leading to a drastic change in the band gap even in the presence of small Fe quantities. The band gap changes abruptly initially as the Fe^{3+} concentration increases, followed by a steadier decrease at high concentrations.[44] A similar situation was observed in $Cs_2Ag_xNa_{1-x}Fe_yIn_{1-y}Cl_6$. The direct band gap drops from 3.10 eV for undoped $Cs_2Ag_xNa_{1-x}InCl_6$ to 1.95 eV for $Cs_2Ag_xNa_{1-x}Fe_{0.99}In_{0.01}Cl_6$.[45] The band gap shows two distinct modes: a slow increase from 1.95 eV to 2.33 eV for $y = 0.99-0.50$, and a steep rise from 2.33 eV to 3.10 eV for $y = 0.50-0.0$ (Fig. 3a).[45] This nonlinear variation of the band gap depending on the composition commonly referred to as the "bowing effect" can be explained by local distortions in the structure. The non-linearly varying band gap is observed in a wide range of semiconducting alloys, including lead and tin halide perovskites.[46–50] Among other factors, local structural relaxations and distortions are shown to be one of the primary reasons for nonlinear changing of the band gap in perovskite systems.[49] A solid-state NMR study shows that Fe^{3+} replaces In^{3+} in the lattice, forming $[FeCl_6]^{3-}\cdot[AgCl_6]^{5-}$ domains with different sizes and distribution modes depending on x, growing larger as the Fe^{3+} concentration increases.[51] This leads to the formation of microscopically segregated Fe^{3+} rich phases in $Cs_2AgIn_xFe_{1-x}Cl_6$ (Fig. 3b).[51]

Transition metal incorporation into a HDP matrix can also change the nature of the band gap by altering the CBM or VBM. In $Cs_2AgBiBr_6$, the substitution of Bi^{3+} with Fe^{3+} leads to a red shift of the absorption onset from 2.1 to $\approx$1 eV due to the lowering of the conduction band minimum by Fe-3d states.[52] DFT calculations explained the band gap reduction and predicted a change from an indirect band gap to a direct band gap for high Fe^{3+} concentrations ($x > 0.5$). After the incorporation of Fe^{3+}, the VBM is mainly derived from Bi-6s and Ag-4d states, while the CBM has an Fe-3d character.[52] The hybridization of Fe-3d and Ag-5s states increases with x, leading to a more dispersed CBM. While the band gap of the pristine compound is indirect, with the VBM and CBM at the Γ and L points, increasing the Fe^{3+} concentration gradually shifts the CBM to X and then to Γ, resulting in a direct band gap for $x > 0.5$.[52] Similar band gap reduction and valence band change were observed in the $Cs_2NaBi_{1-x}Fe_xCl_6$ double perovskite with the incorporation of Fe^{3+} ions into the $Cs_2NaBiCl_6$ lattice.[53] The same effect was achieved through doping with another TM cation, Mn^{2+}. In $Cs_2NaInCl_6$ doped with Mn^{2+}, a slight increase in the band gap is observed and it varies as 4.08, 4.10, 4.11 and 4.12 eV for 0.2, 0.6, 1.1 and 1.7 at% Mn^{2+} respectively.[54] The increase in the band gap is due to the reduced contribution of In-5s at the conduction band maximum caused by the introduction of Mn-3d states.[54]
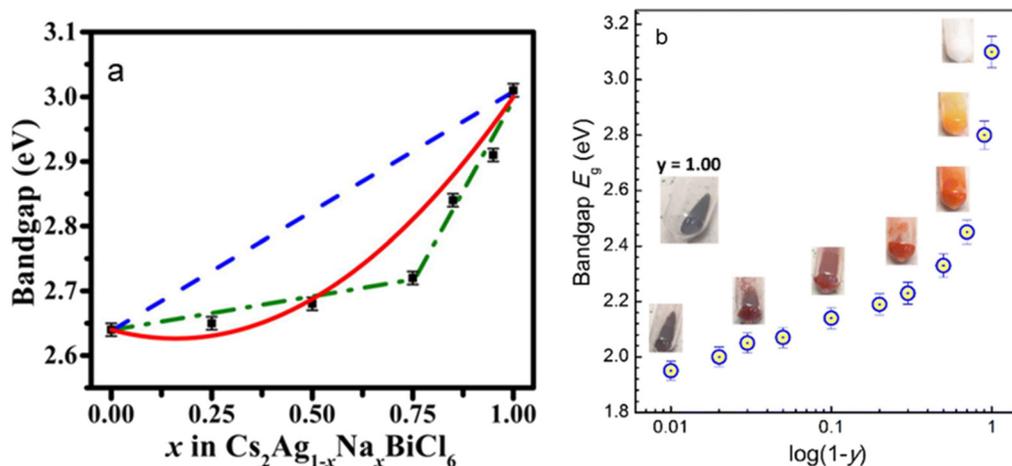

Fig. 3 (a) Band gap variation as a function of the Na content in $Cs_2Ag_{1-x}Na_xBiCl_6$. The black squares are the data points, the dashed blue line shows the band gap predicted by Vegard's law, and the red line is a fit according to the band gap bowing equation. Reproduced from ref. 55 with permission from the American Institute of Physics (AIP). (b) Nonlinear band gap variation in $Cs_2Ag_{1-x}Na_xFe_yIn_{1-y}Cl_6$ as a function of the In content ($1 - y$). Reproduced from ref. 45 with permission from the Royal Society of Chemistry.

Although the trivalent cation site offers more versatility for substitution, Ag/Na substitution has its own distinct effects on the band structure of HDPs. In $Cs_2Ag_{1-x}Na_xBiCl_6$, the band gap changes from 2.64 eV to 3.01 eV as Ag^+ is replaced with Na^+.[55] This change originates primarily from the local distortions of the $[BiCl_6]^{3-}$ and $[AgCl_6]^{5-}$ octahedra, which affect the electronic structure and the interplay between the Ag^+/Na^+ and Bi^{3+} sublattices.[55] The incorporation of silver ions into the sodium site in $Cs_2Ag_xNa_{1-x}BiCl_6$ not only results in a decrease in the lattice parameter, but also introduces covalency through the Ag–Cl bonds. This leads to a strain in the host crystal structure and a variation of the band gap with composition. The band gap deviates from Vegard's rule and shows a "bowing effect".[55] The VBM is mainly formed by the Ag-4d and Cl-3p atomic orbitals, while the CBM is dominated by the Bi-6p and Cl-3p orbitals. As the silver content increases, the Ag-4d states influence the orbital interactions responsible for forming the valence band edge and shift it closer to the Fermi energy.[55] Scanning tunneling spectroscopy studies reveal that the double perovskite alloys form an internal type-I band alignment between the two endmembers, $Cs_2NaBiCl_6$ and $Cs_2AgBiCl_6$.[56] This means that the band gap of an intermediate alloy arises from the lower of the two conduction band edges and the higher of the two valence band edges. This also contributes to the band gap bowing phenomenon.[56] The direct band gap of $Cs_2Ag_xNa_{1-x}Fe_yIn_{1-y}Cl_6$ perovskites also changes with the Ag-to-Na ratio x, which can be varied in the range of 0.1–0.2 < x < 0.6–0.7. The band gap decreases from 2.28 eV for $x = 0.12$ to 1.95 eV for $x = 0.50$ and shows a linear dependence on the actual Ag content x.[45]

Overall, doping and alloying offer versatile routes for band gap engineering in HDP materials. From the present data, one can surmise that the "bowing effect" manifests itself depending on the local structure of the double perovskite. A uniform distribution of dopant atoms in the structure is likely to foster a linear change in the band gap by gradually changing the band structure. However, any local domains or inhomogeneities can result in a type-I internal band alignment and introduce nonlinearity into the change of the electronic properties of the HDP materials.

3. HDP photoluminescence

Photoluminescence of HDPs depends strongly on their composition and electronic structure. Pristine, undoped 3D HDPs often exhibit low PLQYs due to a large indirect band gap, as in $Cs_2AgBiBr_6$ and $Cs_2AgBiCl_6$,[10] or parity forbidden transitions, as in $Cs_2AgInCl_6$.[37] Unlike their 3D counterparts, vacancy-ordered 0D double perovskites (Fig. 4) often demonstrate intrinsic broad band blue-white emission with high PLQYs originating from self-trapped excitons.[17,57] For example, the PLQY of the Rb_2ZrCl_6 phase is 60%.[57] The DFT calculations showed that this compound has a direct band gap of 3.59 eV and electronic states highly localized within the $[ZrCl_6]^{2-}$ units. These PL properties can be tuned by changing the composition of this compound as Cl^- replacement for Br^- in the $Rb_2ZrCl_{6-x}Br_x$ ($0 \leq x \leq 4$) series allowed a 70 nm red shift of the PL peak, while preserving a relatively high PLQY.[57]
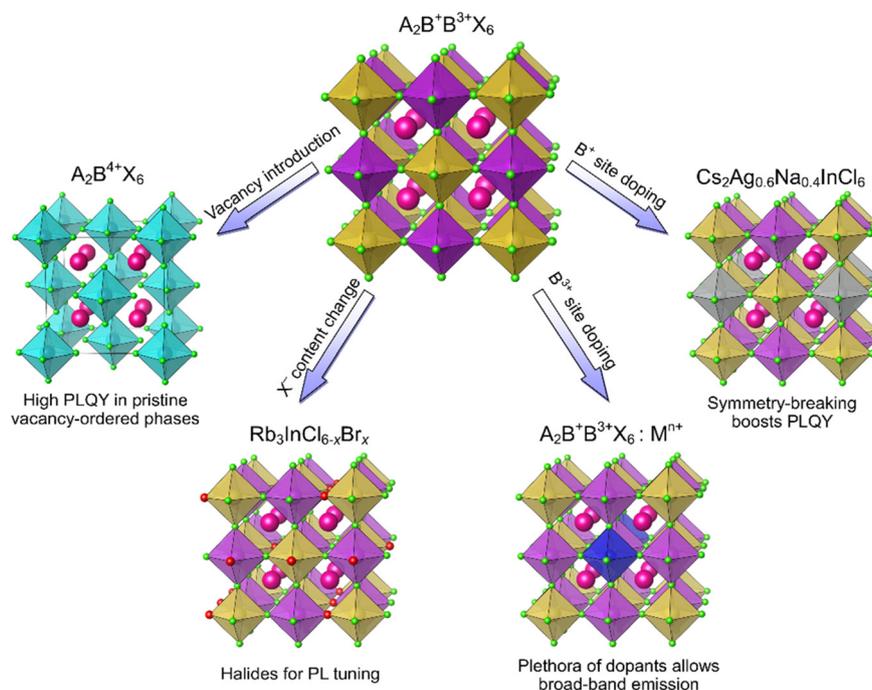

Fig. 4 Compositional changes of HDPs for light conversion applications.

While vacancy-ordered HDPs often offer exceptional PL properties, further enhancement can be achieved through RE incorporation. RE^{3+} cations feature prominent narrow emission bands in specific spectral regions.[58,59] Moreover, while many materials undergo thermal quenching of luminescence, the emission of RE^{3+} originating from f–f transitions shows high thermal stability.[58,59] Since the operation of LEDs unavoidably causes device heating, it is vital for phosphors to sustain the efficiency and color of emitted light at elevated temperatures. For example, a high PLQY of 62% and antithermal quenching of PL in the red and IR regions were reported in $Cs_2NaEr_{0.4}Yb_{0.6}Cl_6$.[60] In this material, a cross relaxation from Er^{3+} to Yb^{3+} excited states results in a peak PL intensity at 400 K, showing a synergistic property enhancement by using two different RE cations.[60]

Although most phosphor converted wLEDs are based on down-conversion of UV or blue radiation from a semiconductor chip by a luminescent material,[61] HDPs doped with RE^{3+} cations offer up-conversion of the IR radiation to visible light. Thus, the pristine $Cs_2NaErCl_6$ HDP exhibits a bright green and orange emission upon IR excitation.[62] The introduction of Yb^{3+} cations into the Er^{3+} sites accentuates and blue shifts the orange emission. Similarly, doping of the $Cs_2NaErCl_6$ phase with Tm^{3+} enhances red emission under 980 nm laser excitation. Efficient up- and down-conversion can be achieved in one material. The Yb^{3+} and Er^{3+} co-doped $Cs_2NaScCl_6$ HDP up-converts 980 and 1550 nm IR laser radiation into green light and down-converts 365 nm UV lamp radiation into red light.[63] Additionally, the material response to the external stimuli depends on the excitation laser power: by increasing the optical power density, the green emission can be redshifted to a yellow one. Multicolor emission achieved in $Cs_2NaErCl_6$ and $Cs_2NaScCl_6$ samples offers advanced anticounterfeiting technologies.[63]

Apart from the significant effect of transition metal doping on the electronic structure, described in the first part of this paper, TM cations also serve as common activators for PL applications.[64] Naturally, they were probed as luminescence centers for HDPs to achieve a remarkable PL. The $Cs_2NaBiCl_6$ double perovskite phosphor demonstrates orange-red emission upon Mn^{2+} doping.[65,66] Noteworthily, a high PLQY (31.6%) and good thermal stability of the emission were achieved by morphology manipulation of the doped material.[66] Another crucial application of $Cs_2NaBiCl_6$:Mn^{2+} is radiation detection. A scintillator film based on $Cs_2NaBiCl_6$:4.04%Mn^{2+} nanocrystals has a high light yield, low detection limits, good spatial resolution and X-ray exposure stability.[67] Doping of the $Cs_2NaBiCl_6$ double perovskite matrix with Mn^{2+} raises some questions on the dopant location in the crystal structure, since there are no 2+ cation positions in the pristine crystal structure; yet charge balance should be achieved somehow. The issue is complicated with typically low concentrations of the dopant, having a negligible effect on the crystal structure. This matter was addressed by a comprehensive magnetic resonance spectroscopy study,[68] which revealed that Mn^{2+} is located in a nearly perfect octahedral Cl^- environment, likely replacing Bi^{3+}.

The reports on ns^2 elements (Sb^{3+}, Te^{4+} and Bi^{3+}) as dopants for halide double perovskites are numerous. These elements are used not only to decrease the band gap, but also to achieve broad-band emission originating in self-trapped exciton recombination. Bright orange emission at 628 nm was reported in Sb^{3+} doped $Rb_3BiCl_6{\cdot}0.5H_2O$.[69] In contrast, the introduction of Sb^{3+} into the $Cs_2Na(Bi, Sb)Cl_6$ structure resulted in a PL peak in the blue-green region (480 nm), while the pristine host material emits orange-red light with a peak at 700 nm.[70] In $Cs_2MInCl_6{:}xSb^{3+}$, the emission color changes from blue to green for M = Na and M = K, respectively.[71] The difference is associated with changes in the crystal structure: the Cs_2KInCl_6 compound is tetragonal, while $Cs_2NaInCl_6$ is cubic.

A remarkable feature of ns^2-doped phases is a wide emission range that covers the entire visible spectra. Tunable white light emission from $Cs_2Zr_{1-x}Te_xCl_6$ solid solutions was reported.[72] While Cs_2TeCl_6 has a low PLQY ($\approx$4%), $Cs_2Zr_{1-x}Te_xCl_6$ ($x = 0.0021$) demonstrates 61.5 and 96.1% PLQYs at 254 and 365 nm excitation, respectively. By doping the Rb_2SnCl_6 matrix with Bi^{3+}, Te^{4+}, and Sb^{3+}, a single component white emitting phosphor has been prepared.[73] This material exhibits bright PL under 365 nm excitation that corresponds to the blue, yellow, and red emission maxima of Bi^{3+}, Te^{4+}, and Sb^{3+} centers, respectively. The combination of yellow and blue emission produces cold white light and is currently employed in wLEDs[61] featuring a Ce^{3+} doped garnet yellow phosphor[74] and a blue emitting InGaN chip.[75] Thus, a wLED employing a 370 nm chip and Rb_2SnCl_6:Bi^{3+},Te^{4+} phosphors with optimized composition achieved a 92.2 color rendering index.[73]

Co-doping of halide double perovskites with various combinations of TM, ns^2, and RE cations is a convenient way to achieve multicolor emission (Fig. 5). If energy transfer between various dopants is allowed, additional effects may appear in their optical behavior. Co-doping of the $Cs_3Cd_2Cl_7$ phase with Mn^{2+} and Sb^{3+} resulted in a long afterglow (over 10 s) in the material.[76] After studying single Mn^{2+} and Sb^{3+} doped $Cs_3Cd_2Cl_7$, the authors concluded that energy transfer occurs from Cd^{2+} to Sb^{3+} and then to Mn^{2+} states. The orange-yellow emission of $Cs_3Cd_2Cl_7$:Mn^{2+},Sb^{3+} originates in d–d relaxations of the Mn^{2+} cation.[76] It is worth noting that the single Mn^{2+} doped phase shows a much higher PLQY, compared to the co-doped phase.[76] In contrast, Cs_2ZnCl_4:Mn^{2+},Sb^{3+} did not show any evidence of charge transfer: the emission of this phase consists of two separate bands which have different excitation energies. Additionally, time-resolved PL showed a single exponential decay behavior for both Mn^{2+} and Sb^{3+} emission.[77] Energy transfer between the dopants was observed for the $Cs_2NaInCl_6$:RE^{3+},Sb^{3+} HDP.[78] $Cs_2NaInCl_6$:Er^{3+},Sb^{3+} emits light in quite separated regions of the spectra – blue and near infrared.[78] On the other hand, no infrared emission was reported for $Cs_2NaInCl_6$:Er^{3+},Ho^{3+},Sb^{3+} and red emission was assigned to Ho^{3+} rather than Er^{3+} cations.[79]

Additionally, doping can cause indirect effects on PL as it occurs in the case of Na^+ doping on the Ag^+ sites in chloride
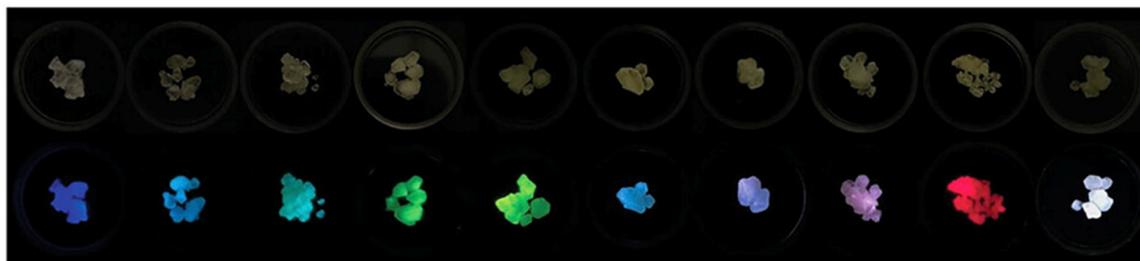
Fig. 5 Sb^{3+} and RE^{3+} co-doped Cs_2NaYCl_6 crystals under visible (top) and UV light (365 nm, bottom). Changing the doping level allows tunable emission. Reproduced from ref. 80 with permission from Wiley-VCH GmbH.

double perovskites. Such doping causes wavefunction symmetry-breaking of the Jahn–Teller distorted $AgCl_6$ octahedra and promotes radiative recombination, which are parity-forbidden in undoped materials.[81] This results in a tremendous improvement of the PLQY from STE emission and was demonstrated for the $Cs_2Ag_{0.60}Na_{0.40}InCl_6:Bi^{3+}$ double perovskite and confirmed later for many mixed Ag/Na phases.[81]

Another intriguing case of broadband emission in halide perovskites requires consideration. In the $Rb_3InCl_{6-x}Br_x$ ($x = 0$, 2, 3, 4, 6) series, the change of the halogen content allowed tuning of the PL wavelength from 436 nm in pure chloride to 505 nm in pure bromide.[82]

Thus, halide double perovskites possess great capabilities for solid state lighting. The unsatisfactory efficiency of pristine materials can be extensively improved by various doping strategies. Co-doping with numerous combinations of ns^2, TM, and RE cations allows achieving broad-band emission in a single matrix. However, the energy transfer between various co-dopants showed a negative effect on the material PLQY in some cases.

4. Conclusions and outlook

The $A_2M'^+M''^{3+}X_6$ double perovskite matrix offers a wide range of compositions as M''^{3+} sites can be occupied by group 13–15 elements, transition metals, rare-earth cations, and combinations thereof. This flexibility provides HDPs with a high degree of tunability of physical properties through various doping and alloying strategies. Isovalent substitution in the series of solid solutions is employed to tune the band gap while preserving its nature. On the other hand, aliovalent substitution introduces new bands in the band structure and shifts the Fermi level more dramatically, oftentimes changing the nature of the band gap. This conversion of an indirect band gap material into a direct one can substantially boost its PLQY. Besides the band structure tuning, the introduction of rare earth, transition metal, or main group cations into HDP matrices produces luminescent materials with the dopant ions acting as luminescence centers. The HDP matrix allows combining various activators, for example, RE^{3+} and Sb^{3+}, to achieve a tunable or broadband emission in a single compound.

Despite the tunability of the composition and properties, HDP materials still face notable limitations. For now, photovoltaic applications of HDPs are challenged by the nature and widths of their band gaps. Most of the materials reported to date are chlorides and bromides with intrinsically larger band gaps, while reports on lower band gap iodides are scarce.[83] Similar to lead perovskites, organic cations such as methylammonium can be employed for the synthesis of hybrid HDP-inspired materials. However, the reduction of the metal halide polyhedra connectivity and formation of low dimension structures often caused by organic cations harm photovoltaic performance.[84]

Overall, lead-free HDP materials offer a non-toxic and stable alternative to lead-based perovskites. Doping and alloying of HDP matrices grant them valuable optical properties. Potential applications of HDPs include phosphor-converted LEDs, anti-counterfeiting technologies and IR detection, while further expansion of their application into lasers and ionizing radiation detection fields can be expected.

Data availability

No primary research results, software or code have been included and no new data were generated or analysed as part of this review.

Author contributions

Sergei A. Novikov – conceptualization, visualization, writing – original draft, and writing – review and editing. Aleksandra D. Valueva – conceptualization, visualization, writing – original draft, and writing – review and editing. Vladislav V. Klepov – conceptualization, funding acquisition, project administration, validation, resources, supervision, and writing – review and editing.

Conflicts of interest

The authors declare no conflict of interest.

Acknowledgements

References

1 Y. Zhao, K. Cruse, M. Abdelsamie, G. Ceder and C. M. Sutter-Fella, *Matter*, 2021, **4**, 1801–1831.
2 A. Bibi, I. Lee, Y. Nah, O. Allam, H. Kim, L. N. Quan, J. Tang, A. Walsh, S. S. Jang, E. H. Sargent and D. H. Kim, *Mater. Today*, 2021, **49**, 123–144.
3 S. Ghosh, H. Shankar and P. Kar, *Mater. Adv.*, 2022, **3**, 3742–3765.
4 S. A. Khan, N. Z. Khan, M. Sohail, M. Runowski, X. Xu and S. Agathopoulos, *Mater. Today Phys.*, 2023, **34**, 101079.
5 A. S. Darsan and A. Pandikumar, *Mater. Sci. Semicond. Process.*, 2024, **174**, 108203.
6 D. Y. Heo, M. A. Tekalgne and S. Y. Kim, *EES Catal.*, 2024, **2**, 94–108.
7 S. Mei, J. Yin, Y. Xing, H. He, H. Gu, J. Xia, W. Zhang, C. Liang, G. Xing and R. Guo, *Nano Energy*, 2024, **122**, 109339.
8 E. T. McClure, M. R. Ball, W. Windl and P. M. Woodward, *Chem. Mater.*, 2016, **28**, 1348–1354.
9 S. J. Zelewski, J. M. Urban, A. Surrente, D. K. Maude, A. Kuc, L. Schade, R. D. Johnson, M. Dollmann, P. K. Nayak, H. J. Snaith, P. Radaelli, R. Kudrawiec, R. J. Nicholas, P. Plochocka and M. Baranowski, *J. Mater. Chem. C*, 2019, **7**, 8350–8356.
10 M. R. Filip, S. Hillman, A. A. Haghighirad, H. J. Snaith and F. Giustino, *J. Phys. Chem. Lett.*, 2016, **7**, 2579–2585.
11 F. Ji, G. Boschloo, F. Wang and F. Gao, *Sol. RRL*, 2023, **7**, 2201112.
12 J. Nie, H. Li, S. Fang, B. Zhou, Z. Liu, F. Chen, Y. Wang and Y. Shi, *Cell Rep. Phys. Sci.*, 2022, **3**, 100820.
13 G. Zhang, D. Wang, B. Lou, C.-G. Ma, A. Meijerink and Y. Wang, *Angew. Chem., Int. Ed.*, 2022, **61**, e202207454.
14 A. Huang, M. Liu, C.-K. Duan, K.-L. Wong and P. A. Tanner, *Inorg. Chem. Front.*, 2022, **9**, 6379–6390.
15 W. Zhuang, H. Liu, Y. Chen, W. Xu, H. Gao, Y. Tian, D. Yao and H. Zhang, *Ceram. Int.*, 2023, **49**, 15761–15770.
16 W. Zhou, C. Li, T. Wu, R. Liu, Z. Ding, R. Zhang, Y. Yu, P. Han and R. Lu, *J. Phys. Chem. Lett.*, 2023, **14**, 8577–8583.
17 K. Zheng, B. Chen, L. Xie, X. Li, B. Lu, M. Wang, Y. Wu, T. Jiang, F. Zhang, X. Li and Y. Wang, *Adv. Opt. Mater.*, 2022, **10**, 2101661.
18 F. Zhu, Y. Gao, C. Zhao, J. Pi and J. Qiu, *ACS Appl. Mater. Interfaces*, 2023, **15**, 39550–39558.
19 M. Jeevaraj, D. Sivaganesh, S. Saravanakumar, S. A. Bahadur, S. Sudhahar and M. K. Kumar, *Opt. Mater.*, 2023, **143**, 114294.
20 C. Zhou, Y. Tian, Z. Yuan, H. Lin, B. Chen, R. Clark, T. Dilbeck, Y. Zhou, J. Hurley, J. Neu, T. Besara, T. Siegrist, P. Djurovich and B. Ma, *ACS Appl. Mater. Interfaces*, 2017, **9**, 44579–44583.
21 A. Žukauskas, R. Vaicekauskas and M. Shur, *Opt. Express*, 2010, **18**, 2287–2295.
22 W. Zhang, S. Thapa, Y. Sun, S. Norville, H. Zhu, P. Zhu, G. Wang and W. Qin, *Chem. Eng. J.*, 2021, **423**, 130186.
23 T. Bai, X. Wang, Z. Wang, S. Ji, X. Meng, Q. Wang, R. Zhang, P. Han, K. Han, J. Chen, F. Liu and B. Yang, *Angew. Chem., Int. Ed.*, 2023, **62**, e202213240.
24 F. Igbari, Z.-K. Wang and L.-S. Liao, *Adv. Energy Mater.*, 2019, **9**, 1803150.
25 L. Lu, X. Pan, J. Luo and Z. Sun, *Chem. – Eur. J.*, 2020, **26**, 16975–16984.
26 Y. Wu, X. Li and H. Zeng, *Small Struct.*, 2021, **2**, 2000071.
27 T. Appadurai, R. Kashikar, P. Sikarwar, S. Antharjanam, B. R. K. Nanda and A. K. Chandiran, *Commun. Mater.*, 2021, **2**, 1–16.
28 L. Zhang and M. Yuan, *Light: Sci. Appl.*, 2022, **11**, 99.
29 T. Wang, D. Zhou, Z. Yu, T. Zhou, R. Sun, Y. Wang, X. Sun, Y. Wang, Y. Shao and H. Song, *Energy Mater. Adv.*, 2023, **4**, 0024.
30 S. Jin, R. Li, H. Huang, N. Jiang, J. Lin, S. Wang, Y. Zheng, X. Chen and D. Chen, *Light: Sci. Appl.*, 2022, **11**, 52.
31 R. Zhang, Z. Wang, X. Xu, X. Mao, J. Xiong, Y. Yang and K. Han, *Adv. Opt. Mater.*, 2021, **9**, 2100689.
32 S. Li, C. Zhu, J. Wang, Z. Zhang, D. Wang, Y. Chen, D. Zhang, J. Wang and J. Zhang, *J. Mater. Chem. C*, 2024, **12**, 4720–4727.
33 X. Deng, S. Cheng, X. Chen, M. Wang, X. Li, G. Li, D. Zhu, M. Jia, X. Li and Z. Shi, *J. Lumin.*, 2024, **269**, 120525.
34 Y. Zhang, X. Liu, H. Sun, J. Zhang, X. Gao, C. Yang, Q. Li, H. Jiang, J. Wang and D. Xu, *Angew. Chem., Int. Ed.*, 2021, **60**, 7587–7592.
35 X. Cheng, Z. Xie, W. Zheng, R. Li, Z. Deng, D. Tu, X. Shang, J. Xu, Z. Gong, X. Li and X. Chen, *Adv. Sci.*, 2022, **9**, 2103724.
36 A. A. Bhat, N. Singh, R. V. Nair, E. Dujardin and J. Sharma, *Opt. Mater.*, 2023, **141**, 113937.
37 W. Meng, X. Wang, Z. Xiao, J. Wang, D. B. Mitzi and Y. Yan, *J. Phys. Chem. Lett.*, 2017, **8**, 2999–3007.
38 S. Yoon, B. Fett, A. Frebel, S. Kroisl, B. Herbig, M. Widenmeyer, B. Balke, G. Sextl, K. Mandel and A. Weidenkaff, *Energy Technol.*, 2022, **10**, 2200197.
39 P. Sebastiá-Luna, J. Calbo, N. Albiach-Sebastián, M. Sessolo, F. Palazón, E. Ortí and H. J. Bolink, *Chem. Mater.*, 2021, **33**, 8028–8035.
40 Y. Liu, X. Dai, X. Zeng, X. Yuan, Y. Wang, Y. Song, H. Chen, C. Zhang, Y. Wang, L. Wan, Y. Zou, W. Ning and B. Sun, *Adv. Opt. Mater.*, 2024, **12**, 2301576.
41 Z. Xiao, *Adv. Opt. Mater.*, 2024, 2302471.
42 O. Stroyuk, O. Raievska, A. Barabash, C. Kupfer, A. Osvet, V. Dzhagan, D. R. T. Zahn, J. Hauch and C. J. Brabec, *Mater. Adv.*, 2022, **3**, 7894–7903.
43 Z. Zhang, G. Liu, W. Guo, X. Li, Y. Zhang, C. Wu, B. Qu, J. Shi, Z. Chen and L. Xiao, *Mater. Adv.*, 2022, **3**, 4932–4937.

44 H. Yin, Y. Xian, Y. Zhang, W. Chen, X. Wen, N. U. Rahman, Y. Long, B. Jia, J. Fan and W. Li, *Adv. Funct. Mater.*, 2020, **30**, 2002225.

45 O. Stroyuk, O. Raievska, A. Barabash, J. Hauch and C. J. Brabec, *J. Mater. Chem. C*, 2023, **11**, 6867–6873.

46 S.-H. Wei and A. Zunger, *Phys. Rev. B: Condens. Matter Mater. Phys.*, 1989, **39**, 3279–3304.

47 W. Shan, W. Walukiewicz, J. W. Ager, E. E. Haller, J. F. Geisz, D. J. Friedman, J. M. Olson and S. R. Kurtz, *Phys. Rev. Lett.*, 1999, **82**, 1221–1224.

48 J. Wu, W. Walukiewicz, K. M. Yu, J. W. Ager, E. E. Haller, I. Miotkowski, A. K. Ramdas, C.-H. Su, I. K. Sou, R. C. C. Perera and J. D. Denlinger, *Phys. Rev. B: Condens. Matter Mater. Phys.*, 2003, **67**, 035207.

49 A. Rajagopal, R. J. Stoddard, H. W. Hillhouse and A. K.-Y. Jen, *J. Mater. Chem. A*, 2019, **7**, 16285–16293.

50 S. Khatun, A. Maiti and A. J. Pal, *Appl. Phys. Lett.*, 2020, **116**, 012104.

51 F. Ji, F. Wang, L. Kobera, S. Abbrent, J. Brus, W. Ning and F. Gao, *Chem. Sci.*, 2021, **12**, 1730–1735.

52 H. J. Jöbsis, K. Fykouras, J. W. C. Reinders, J. van Katwijk, J. M. Dorresteijn, T. Arens, I. Vollmer, L. A. Muscarella, L. Leppert and E. M. Hutter, *Adv. Funct. Mater.* 2306106.

53 R. Udavant, S. Thawarkar, S. Rondiya, A. Shelke, R. Aher, T. G. Ajithkumar, R. W. Cross, N. Y. Dzade and S. Jadkar, *Inorg. Chem.*, 2023, **62**, 4861–4871.

54 M. Jeevaraj, D. Sivaganesh, S. Saravanakumar, S. A. Bahadur, S. Sudhahar and M. K. Kumar, *Mater. Chem. Phys.*, 2024, **311**, 128569.

55 A. C. Dakshinamurthy and C. Sudakar, *Appl. Phys. Lett.*, 2021, **118**, 131902.

56 S. Dan, A. Maiti, S. Chatterjee and A. J. Pal, *J. Phys.: Condens. Matter*, 2021, **33**, 485701.

57 F. Zhang, Z. Chen, Z. Liu, M. Jia, X. Chen, D. Wu, X. Li and Z. Shi, *J. Lumin.*, 2022, **251**, 119150.

58 *Luminescence: from theory to applications*, ed. C. R. Ronda, Wiley-VCH, Weinheim, 2008.

59 *Luminescence: Theory and Applications of Rare Earth Activated Phosphors*, ed. R. Tiwari, V. Dubey, V. Singh and M. E. Z. Saucedo, De Gruyter, 2021.

60 G. Zhang, P. Dang, H. Lian, H. Xiao, Z. Cheng and J. Lin, *Laser Photonics Rev.*, 2022, **16**, 2200078.

61 D. A. Steigerwald, J. C. Bhat, D. Collins, R. M. Fletcher, M. O. Holcomb, M. J. Ludowise, P. S. Martin and S. L. Rudaz, *IEEE J. Sel. Top. Quantum Electron.*, 2002, **8**, 310–320.

62 G. Zhang, P. Dang, H. Lian, S. Huang, W. Yang, Z. Cheng and J. Lin, *Adv. Opt. Mater.*, 2022, **10**, 2201220.

63 R. Gao, C. Chen, M. Jin, J. Xiang, Z. Li, R. Chen, N. Zhang and C. Guo, *Mater. Res. Bull.*, 2024, **172**, 112651.

64 V. Rajendran, H. Chang and R.-S. Liu, in *Transition metal ion-based phosphors for LED applications*, De Gruyter, 2023, ch. 8, pp. 185–220.

65 M. Jeevaraj, S. Sudhahar, P. Devendran, N. Nallamuthu, N. D. Jayram and M. K. Kumar, *Mater. Today Commun.*, 2022, **33**, 104715.

66 S. Fang, T. Wang, S. He, T. Han, M. Cai, B. Liu, V. I. Korepanov and T. Lang, *Phys. Chem. Chem. Phys.*, 2022, **24**, 9866–9874.

67 N. Varnakavi, R. Rajavaram, K. Gupta, P.-R. Cha and N. Lee, *Adv. Opt. Mater.*, 2023, 2301868.

68 A. Karmakar, G. M. Bernard, A. Pominov, T. Tabassum, R. Chaklashiya, S. Han, S. K. Jain and V. K. Michaelis, *J. Am. Chem. Soc.*, 2023, **145**, 4485–4499.

69 Z. Jia, P. Gong, M. Chen, Z. Wang, X. Li, Y. Song, S. Zhang, N. Zhang and M. Xia, *Inorg. Chem.*, 2023, **62**, 19690–19697.

70 S. Wu, W. Li, J. Hu and P. Gao, *J. Mater. Chem. C*, 2020, **8**, 13603–13611.

71 A. Noculak, V. Morad, K. M. McCall, S. Yakunin, Y. Shynkarenko, M. Wörle and M. V. Kovalenko, *Chem. Mater.*, 2020, **32**, 5118–5124.

72 Y. Liu, Y. Wu, Z. Juan, X. Sun, W. Zhang, H. Zeng and X. Li, *Adv. Opt. Mater.*, 2021, **9**, 2100815.

73 R. Liu, W. Zhang, T. Wen, X. Wen, C. Ding, Z. Li and W. Yan, *J. Phys. Chem. Lett.*, 2022, **13**, 11143–11152.

74 G. Blasse and A. Bril, *Appl. Phys. Lett.*, 1967, **11**, 53–55.

75 S. Nakamura and G. Fasol, *The Blue Laser Diode: GaN Based Light Emitters and Lasers*, Springer-Verlag, Berlin Heidelberg, 1997.

76 G. Dai, Z. Ma, Y. Qiu and Z. Ma, *Inorg. Chem.*, 2023, **62**, 7906–7913.

77 T. Zheng, H. Yang, Y. Liu, Y. Li, Q. Huang, L. Zhang and X. Li, *Inorg. Chem.*, 2023, **62**, 17352–17361.

78 S. Saikia, A. Joshi, H. Arfin, S. Badola, S. Saha and A. Nag, *Angew. Chem., Int. Ed.*, 2022, **61**, e202201628.

79 J. Nie, B. Zhou, S. Fang, H. Zhong, H. Li and Y. Shi, *Chem. Mater.*, 2022, **34**, 6288–6295.

80 X.-X. Guo, J.-H. Wei, J.-B. Luo, Z.-L. He, Z.-Z. Zhang, J.-H. Chen and D.-B. Kuang, *Adv. Opt. Mater.*, 2023, 2301914.

81 J. Luo, X. Wang, S. Li, J. Liu, Y. Guo, G. Niu, L. Yao, Y. Fu, L. Gao, Q. Dong, C. Zhao, M. Leng, F. Ma, W. Liang, L. Wang, S. Jin, J. Han, L. Zhang, J. Etheridge, J. Wang, Y. Yan, E. H. Sargent and J. Tang, *Nature*, 2018, **563**, 541–545.

82 X. Liu, C. Zhang, Y. Cao, Y. Wang, L. Peng, J. Chen and J. Lin, *Mater. Today Chem.*, 2023, **29**, 101459.

83 P. Vishnoi, R. Seshadri and A. K. Cheetham, *J. Phys. Chem. C*, 2021, **125**, 11756–11764.

84 W. Fu, H. Chen and A. K.-Y. Jen, *Mater. Today Nano*, 2021, **14**, 100117.